ACTIVITY AND KINEMATICS OF WHITE DWARF-M DWARF BINARIES FROM THE SUPERBLINK PROPER MOTION SURVEY[1]

Julie N. Skinner[2], Dylan P. Morgan[3], Andrew A. West[3], Sébastien Lépine[4], John R. Thorstensen[5]

[1]Based on Observations obtained at the MDM Observatory operated by Dartmouth College, Columbia University, The Ohio State University, and the University of Michigan

[2]Institute for Astrophysical Research, Boston University, 725 Commonwealth Avenue, Boston, MA 02215, USA; jskinner@bu.edu

[3]Department of Astronomy, Boston University, 725 Commonwealth Avenue, Boston, MA 02215, USA

[4]Department of Physics & Astronomy, Georgia State University, 25 Park Place NE, Atlanta, GA, 30303, USA

[5]Department of Physics and Astronomy, 6127 Wilder Laboratory, Dartmouth College, Hanover, NH 03755, USA

ABSTRACT

We present an activity and kinematic analysis of high proper motion white dwarf-M dwarf binaries (WD+dMs) found in the SUPERBLINK proper motion survey ($\mu > 40$ mas yr^{-1}), 178 of which are new identifications. To identify WD+dMs in SUPERBLINK, we developed a UV-optical-IR color criterion and conducted a spectroscopic survey to confirm each candidate binary using the 2.4m Hiltner and the 1.3m McGraw-Hill telescopes at MDM Observatory. For the newly identified systems, we fit the two components using model white dwarf spectra and M dwarf template spectra to determine physical parameters for the individual stars, as well as some system properties. We use Hα chromospheric emission to examine the magnetic activity of the M dwarf in each system, and how magnetic activity is affected by the presence of a white dwarf companion. We find that the fraction of WD+dM binaries with active M dwarfs is significantly higher than their single M dwarf counterparts at early and mid spectral types. We investigate the effects of binary separation on M dwarf activity and corroborate previous studies that find high activity fractions at both close and intermediate separations. We also find enticing evidence of a separation threshold where the binary magnetic activity fraction matches the magnetic activity fraction for single M dwarfs. Using results from our spectroscopic fits and the proper motions from SUPERBLINK, we calculate 3D space velocities for the WD+dMs in SUPERBLINK. For the entire SUPERBLINK sample, we find a large vertical velocity dispersion, indicating a dynamically hotter population compared to high proper motion samples of single M dwarfs. We compare the kinematics for systems with active M dwarfs and those with inactive M dwarfs, and find signatures of asymmetric drift in the inactive sample, indicating that they are drawn from an older population.

1. INTRODUCTION

Low-mass stars are the most populous stellar constituents in our galaxy and are vital to understanding our galaxy's structure and kinematics (Gizis et al. 2002; West et al. 2004; Bochanski et al. 2007a). Over a quarter of low-mass stars are found in binary or higher-order systems (Duchêne & Kraus 2013), making it crucial to understand how binary companions affect low-mass star formation and evolutionary processes. One such process is the evolution of stellar magnetic fields with age and the subsequent change in the magnetic heating of the upper atmosphere. Despite many observations of magnetic activity, the exact mechanism behind chromospheric and coronal heating in low-mass star atmospheres is not well-understood. In solar-type stars, differential rotation between the inner radiative zone and outer convective layer causes rotational shear that organizes and amplifies the magnetic field, with faster rotating stars having stronger magnetic fields. This strong magnetic field provides the energy to heat the stellar chromosphere and corona and gives rise to line emission (as well as continuum), which is used to trace the magnetic activity. Over time, the stellar rotation period decreases due to loss of angular momentum from the magnetized winds leaving the star, linking stellar rotation, age, and magnetic activity.

Previous studies have found that the rotation-activity correlations observed in solar-type stars also apply to early-type M dwarfs (M0-M3; Kiraga & Stepien e.g. 2007). However, around spectral type ∼M4, M dwarfs transition to a fully convective interior (0.35 M$_\odot$; Chabrier & Baraffe 1997) and rotational shear at the tachocline can no longer serve as an explanation for the creation of large scale magnetic fields. Late-type M dwarfs show the observational signatures of strong magnetic activity (Delfosse et al. 1998; Mohanty & Basri 2003; Reiners & Basri 2007), but the full details of the relationship between fully convective stars, rotation, age, and the generation of the magnetic field are not yet fully under-

stood. However, recent work from West et al. (2015) showed that the high activity fraction observed in a sample of late-type M dwarfs persists to shorter rotation periods than for early-type M dwarfs, indicating that rotation is important in these late-type stars and the activity-rotation relation is mass dependent.

Binaries provide a window into the physical characteristics of stars not usually afforded from their single counterparts. Close, interacting systems allow us to better understand accretion properties and mass loss through winds. Wide binary systems with M dwarfs are often used to better understand the abundances and ages of low-mass stars, through a study of their co-eval companions. In addition, if these systems are eclipsing, complete orbital properties can be derived and therefore fundamental stellar parameters can be determined. Eclipsing binaries often act as anchor points for stellar evolution models (Feiden 2015, and references therein), highlighting the importance of understanding at which separations interactions between the stars affect the observed and physical properties of the components. The previous categories of close or wide, while useful, ignores intermediate separations where interaction between the stars may be more subtle. In this work, we will highlight the need to use three categories of binary separation[6] – close (a $\leq$ 0.88 AU), intermediate (0.88 AU < a $\leq$ 2.57 AU), and wide (a > 2.57 AU).

White dwarf-M dwarf binaries (WD+dMs) provide an important laboratory to explore how close companions affect M dwarfs. One advantage of studying WD+dMs is the distinct spectral signature from each star. White dwarfs and M dwarfs have similar luminosities, but differing SEDs, making separation of each component relatively easy. One avenue to examine is how magnetic activity changes due to binary companions. To fully understand the magnetic activity evolution of WD+dMs, it is important to have large, statistically significant samples of these binaries. In recent years, there have been several studies on white dwarf-main sequence binaries (WDMS) primarily identified from the Sloan Digital Sky Survey (SDSS; York et al. 2000). Most recently, Rebassa-Mansergas et al. (2016) presented the updated SDSS DR1-12 spectroscopic catalog of WDMS binaries with 3294 systems. The same team previously employed a two step color selection using both SDSS *ugriz* photometry, as well as a search for infrared excess in the Two Micron All Sky Survey (2MASS; Skrutskie et al. 2006, the Wide-field Infrared Survey Explorer (*WISE*; Wright et al. 2010), and the UK Infrared Telescope (UKIRT) Infrared Sky Survey (Lawrence et al. 2007; Warren et al. 2007; Rebassa-Mansergas et al. 2013a). Other studies utilizing the SDSS catalog include the Silvestri et al. (2006); Heller et al. (2009); Morgan et al. (2012); Liu et al. (2012). Addition-

ally, 121 WDMS binaries were identified from the Large sky Area Multi-Object Spectroscopic Telescope (LAMOST) DR1 (Ren et al. 2014). While all of these studies have significant overlap, Rebassa-Mansergas et al. (2016) presents the largest, homogeneous sample of spectroscopically confirmed WDMS systems. Prior to these larger studies, Raymond et al. (2003) identified $\simeq$ 100 WD+dMs from SDSS and Schreiber & Gänsicke (2003) presented a listing of 30 known PCEBs identified through a variety of methods. In most cases, the WD+dMs in these studies have been selected from SDSS, and are biased against cool white dwarfs or early-type M dwarfs Rebassa-Mansergas et al. (2013a). WD+dMs from SDSS have spectroscopic distances typically greater than a few hundred parsecs, leaving many of the solar neighborhood WD+dMs unidentified. Samples of more nearby WD+dMs, on the other hand, offer the opportunity to study the kinematics of these binaries, as well as the opportunity to build a volume-limited sample of WD+dMs. Surveys of high proper motion stars, like the SUPERBLINK proper motion survey (e.g. Lépine & Gaidos 2011) make it possible to examine these very nearby WD+dMs.

Previous studies examining the activity of M dwarfs with white dwarf companions (Silvestri et al. 2007; Morgan et al. 2012; Rebassa-Mansergas et al. 2013b) have shown that the fraction of active early and mid-type M dwarfs with white dwarf companions is higher than their single counterparts. For late-type M dwarfs, activity fractions for WD+dMs approach similar levels as single M dwarfs, suggesting that angular momentum loss in fully convective single M dwarfs is less efficient than for early and mid-types. Additionally, Morgan et al. (2012) and Rebassa-Mansergas et al. (2013b) found that WD+dMs at intermediate-to-wide separations have higher activity fractions than similar samples of single M dwarfs. Rebassa-Mansergas et al. (2013b) attribute this high activity fraction to the preferential selection of systems with younger, hotter white dwarfs.

Since binaries at different separations inhabit different dynamical regimes, the physical mechanism producing higher magnetic activity fractions in WD+dMs likely varies as a function of binary separation. The closest WD+dMs (P_{orb} $\lesssim$ 10 days, Nebot Gomez-Moran et al. 2011) are products of common envelope evolution, the binary evolution state in which the envelope of the WD progenitor engulfs the companion M dwarf. Binary angular momentum is subsequently extracted to eject the envelope, and a very close WD+dM emerges as a post common-envelope binary or PCEB. In these systems, tidal locking ensures that the M dwarf will be rapidly rotating, and therefore likely observed as active. Rebassa-Mansergas et al. (2013b) found that all of the confirmed PCEBs in their sample were active across all observed M dwarf subtypes (M2-M7). Morgan et al. (2012) also found that the closest WD+dMs (a < 0.1 AU) have high activity fractions across all M dwarf subtypes, while the widest systems (a = 1-100 AU) had low activity fractions at early M

---

[6] These regimes are based on the possible evolution scenarios for white dwarf-main sequence binaries as outlined by Willems & Kolb (2004).

spectral types with an increasing activity fraction toward late spectral types.

WD+dMs at wider separations do not undergo common envelope evolution, and are often assumed to evolve as single stars. However, differences in the lifetime of the circumstellar disk at early epochs may play a significant role in the subsequent angular momentum evolution. To avoid approaching rotation speeds close to the breakup limit, single stars must shed the angular momentum gained during the pre-main-sequence stage. Single stars may dissipate angular momentum through accretion-powered winds (Matt & Pudritz 2005), or through disk locking (Ghosh & Lamb 1979; Shu et al. 1994), which applies a torque on the star through a magnetic bridge between the star and the disk. In binaries, the companion star may disrupt the disk, and thus shorten the time available for either mechanism to carry away angular momentum, resulting in a system that arrives at its post-disk life with a faster rotation period. Meibom et al. (2007) found that the solar-type primary stars of binaries (0.1 AU $\lesssim$ a $\lesssim$ 5 AU) in M35 had faster rotation periods on average than solar-type single stars in the same cluster. The effects disk disruption may have at later times are crucial to understanding the separation threshold at which stars in binaries can be assumed to evolve as single stars (i.e. this assumption may not hold for stars at intermediate separations).

In this paper, we present the sample of WD+dM binaries extracted from the SUPERBLINK proper motion survey. In section 2, we outline our target and color selection, as well as spectroscopic observations from our subsequent, follow-up program. Section 3 outlines our two-component fits to the recorded spectra, as well as the resulting spectroscopic distances and orbital characteristics that we derive from these fits. In section 4, we present the 3D kinematics of this sample and discuss the results of our magnetic activity analysis. Lastly, a summary of the results and concluding remarks are presented in section 5.

2. TARGET SELECTION & OBSERVATIONS

To select for nearby WD+dMs, we used the SUPERBLINK proper motion survey (Lépine et al. 2002; Lépine & Shara 2005), an ongoing all-sky survey which identifies and characterizes stars with proper motions $\mu > 40$ mas yr^{-1}. The SUPERBLINK catalog is assembled from an automated search of the Digitized Sky Surveys (DSS), followed by visual examination of objects flagged with large proper motions. Images from two epochs are aligned and normalized before being differenced to produce a residual image; objects with large proper motions are identified as high intensity pairs on the residual image by the software, and visually checked by blinking the finding charts generated by SUPERBLINK. For this study, we used the July 2011 version of SUPERBLINK, which listed 2,270,481 stars, and was estimated to be >90 % complete to $V = 19.0$. The catalog is known to be more complete at higher galactic latitudes

(>95%) where crowding is minimal, and the low-latitude completeness is estimated to be >80-85%. SUPERBLINK has been cross-matched with photometric archives including the *ROSAT* All-Sky Survey Bright Source Catalog (Voges et al. 1999), the *ROSAT* All-Sky Survey Faint Source Catalog (Voges et al. 2000), the fifth data release from *Galaxy Evolution Explorer* (*GALEX*; Martin et al. 2005), and the Two Micron All Sky Survey (2MASS; Skrutskie et al. 2006) catalog. The astrometric and photometric properties for the SUPERBLINK sample of WD+dMs are shown in Table 1. None of the objects in our sample had X-ray detections from ROSAT, so we have not included those data in the table.

We selected WD+dMs based on a combination of V magnitudes derived from the DSS plates (see Lépine & Shara 2005), near-UV magnitudes from *GALEX*, and K_s magnitudes from 2MASS. Using the UV-optical-IR color-selection outlined in Skinner et al. (2014), we selected targets for spectroscopic follow-up (see Figure 1). We acquired optical spectroscopy of 178 newly identified WD+dM candidates, with the Boller and Chivens CCD spectrograph (CCDS), using both the Hiltner 2.4m and McGraw-Hill 1.3m telescopes located at MDM Observatory. The detector is a Loral 1200 x 800 CCD with several gratings available. For all CCDS spectra, we used the 150 l/mm grating, which is blazed at 4700 Å. With the exception of a portion of the April 2011 observing run, we inserted a LG-350 order blocking filter to block second-order contributions to the spectra. Slit sizes were 1.2-arcsec at the 2.4m and 1.5-arcsec at the 1.3m, which yielded resolutions of 10 Å and 8 Å, respectively. Observing conditions over the multiple runs were varied. Objects confirmed to be WD+dM binaries that were originally observed in poor conditions were typically re-observed in better conditions at a later date.

To maximize efficiency at the telescope, spectra were calibrated using comparison lamp spectra taken during twilight to find the shape of the pixel-to-wavelength relation, then shifts to each spectrum were derived from the 5577 Å night sky line to set the zero-point of the calibration. To confirm that these shifts were applied correctly, the IRAF task *xcsao* was used to cross-correlate the 6100-6700 Å region of each spectrum with an average sky spectrum constructed using a similar instrument. These reductions were done using standard IRAF routines. In addition to our target spectroscopy, we obtained spectra of flux standard stars and well-known M dwarf spectral type standards. The former were used for flux calibration, the latter as templates for spectral typing the M dwarfs discovered in WD+dM systems. In addition, we observed hot O and B stars to correct for telluric absorption.

For many of the WD+dMs that we confirmed from these spectra, we obtained additional optical spectra at longer wavelengths using the 1.3m McGraw-Hill telescope. For this, we used the Mark III Spectrograph and the MDM detector Nellie. Nellie is a STIS 2048^2 thick, frontside illuminated CCD. In all MkIII spectra, we used a 300 l/mm grism
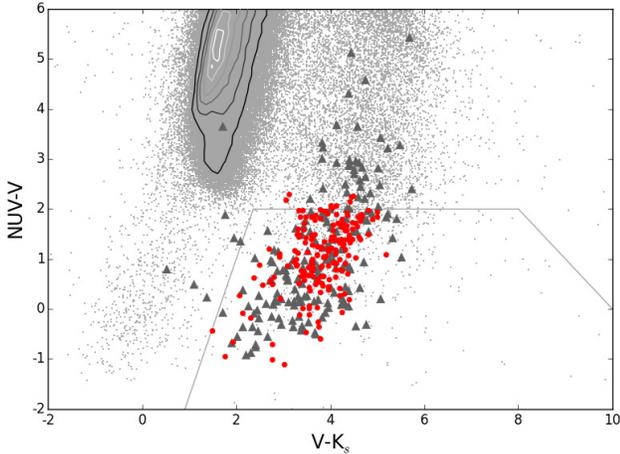
Figure 1. The *NUV-V* and *V-K$_s$* color-color diagram is shown with the SUPERBLINK stars plotted as grey dots. Contours are shown to highlight the main stellar locus. WD+dMs identified in this study are plotted as red dots, and shown to have significant excesses in the near-UV and infrared K. Gray triangles show the previously identified WD+dMs from SDSS (Rebassa-Mansergas et al. 2010) that are recovered in SUPERBLINK. Gray lines indicate our initial color-space selection, from which we conducted our spectroscopic survey. Some previously known WD+dMs fall outside our selection box, indicating that our color selection scheme should be expanded to redder *NUV-V* colors.

blaze at 6400 Å with a Hoya Y-50 order blocking filter with a 1.52-arcsec slit. Reductions were done in the same manner as outlined above. Spectra from CCDS were used for most of the analysis in this paper, but MkIII spectra were used as additional confirmation of M dwarf spectral type when necessary.

3. ANALYSIS

3.1. *Two-Component Fits*

For each of the WD+dM binaries observed, we decomposed each spectrum into the two components with the help of white dwarf model spectra (Koester et al. 2001) and M dwarf templates Bochanski et al. (2007b). Figure 2 shows example spectra with the best-fit model/template combination. To find the best combination, we followed the iterative χ^2-minimization method described in Morgan et al. (2012). Briefly, the full spectrum is fit first with a white dwarf model that is then subtracted from the spectrum. An M dwarf template is then fit to the WD-subtracted spectrum. The process is repeated on the original spectrum, this time fitting the M dwarf template first, then the WD model. As a part of the fitting process, some spectral regimes (e.g. the Balmer lines from the WD) are given greater or lesser weight according to their contribution to the full spectrum. Several iterations of this process are performed until the best-fit WD model and best-fit M dwarf template do not change over multiple iterations. In cases where a solution is not found after 10 iterations, the process is terminated, and the fit with the lowest χ^2 value is chosen. Radial velocities for the both

the WD and M dwarf components are determined by cross-correlating the separated spectra with the corresponding best-fit model or template after each iteration. The radial velocity is then used to obtain a better fit by shifting the templates in subsequent iterations. The WD model atmosphere grid used in this analysis was coarse, and WD fits to a finer grid of models are warranted at a future time. Figure 3 shows the effective temperature, log g, WD mass, M dwarf spectral type, binary separation, and distance for the new WD+dMs found in SUPERBLINK, along with comparisons to the appropriate binary and single star samples. Table 2 gives the results of our two-component fits, as well as the spectroscopic distances (described below) for the newly identified SUPERBLINK WD+dMs.

3.2. *Spectroscopic Distances*

Using the physical parameters derived from our spectroscopic fits, we determined spectroscopic distances to each of the components of the binary. Using the determined effective temperatures and gravities from the WD model fits, we used synthetic color sequences developed by Pierre Bergeron and collaborators[1] (Holberg & Bergeron 2006; Kowalski & Saumon 2006; Tremblay et al. 2011; Bergeron et al. 2011). Interpolating over their grid for M$_{NUV}$ (P. Bergeron, private communication), we determined absolute near-UV magnitudes for the WDs in each of the systems and then calculated distances. For single M dwarfs, photometric distance relationships typically have less scatter than spectral type-absolute magnitude relationships (Bochanski et al. 2011; Lépine et al. 2013). However, for WD+dM systems, the compound colors will not adhere to typical, single M dwarf photometric parallax relations since the white dwarf contributes flux in optical and UV. To minimize contamination from the WD, we used the spectroscopic parallax relation from Lépine et al. (2013) to determine absolute *J-band* magnitudes for the M dwarfs based on their spectral types. Specifically, the relevant relationships for this study are as follows:

$$M_J = 5.220 + 0.393(SpT) + 0.040(SpT)^2$$
$$for\ Active\ K7 - M2.5$$
$$M_J = 5.680 + 0.393(SpT) + 0.040(SpT)^2$$
$$for\ Inactive\ K7 - M6$$

This relationship reflects the fact that active early-type M dwarfs are systematically more luminous than their non-active counterparts (see Bochanski et al. 2011 and references therein). We use the early-active relation for stars with subtype M2.5 and earlier. Uncertainty in the determined M dwarf distances is dominated by the spectral type determination, since the 2MASS *J-band* magnitudes typi-

---

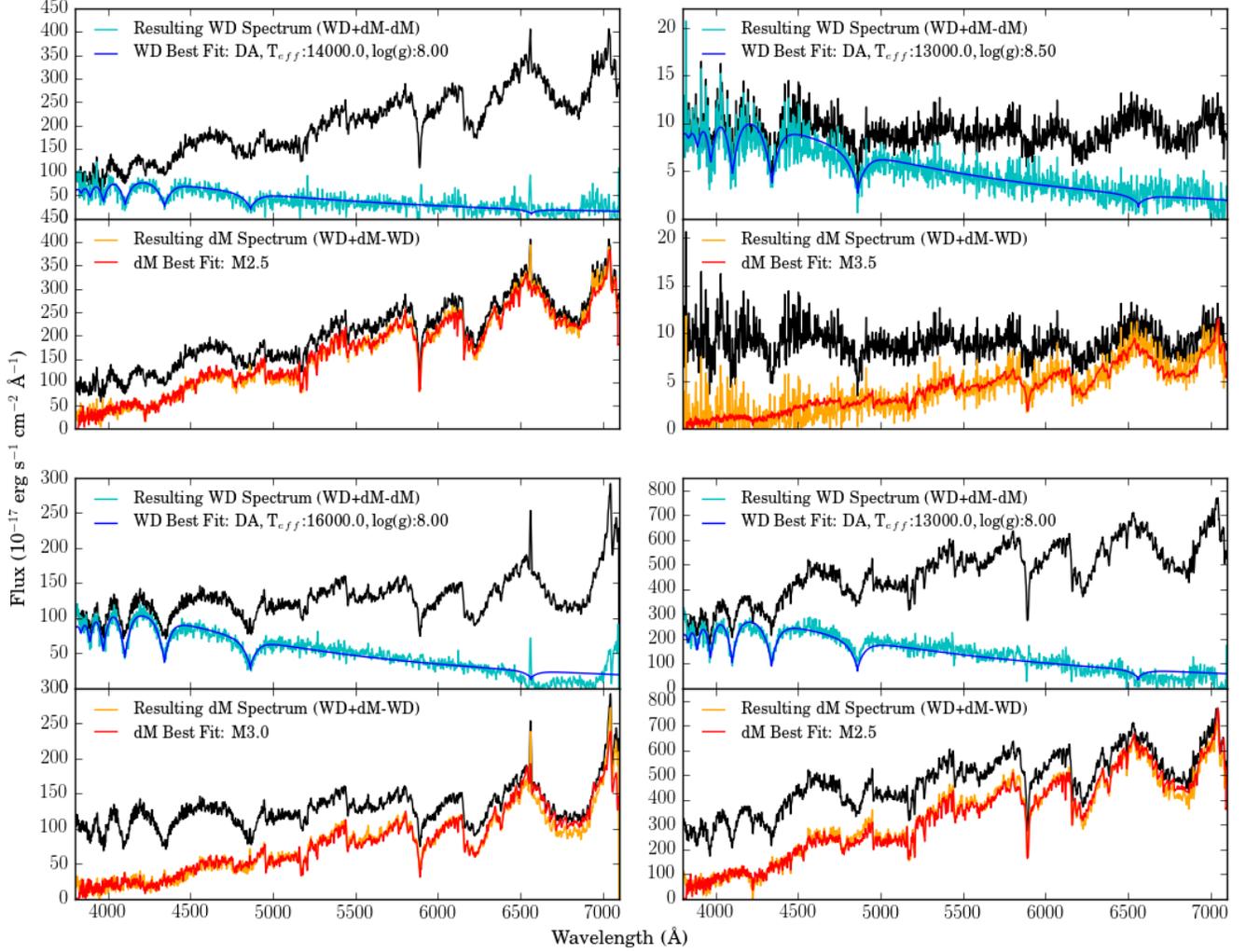[1] http://www.astro.umontreal.ca/~bergeron/CoolingModels/

Figure 2. Examples of our two-component fitting procedure as outlined in Section 3.1. Each of the top panels shows our original spectrum in black, the best-fit model WD spectrum in blue, and the target spectrum with the best-fit M dwarf template subtracted in cyan. Each of the bottom panels shows the original spectrum in black, the best-fit M dwarf template in red, and the target spectrum with the best-fit model WD spectrum subtracted in orange.

cally have small uncertainties. The top panel of Figure 4 compares the two distance determinations made for the sample of WD+dMs from the SUPERBLINK catalog (described below; shown as black dots) and the sample of WD+dMs from SDSS (Rebassa-Mansergas et al. 2013a; shown as grey dots). The bottom panel shows the residual values for the same objects. We estimate that both distance estimates have uncertainties of ∼15%.

3.3. *Orbit Characteristics*

As stated in Section 3.1, we measure radial velocities from our spectra using the cross-correlation of our spectra with the appropriate model or template. White dwarf masses were determined using the photometric calibration models referred to in the previous section. M dwarf masses were assigned based on spectral type using the relation from Reid & Hawley (2005). Each of the measured velocities (v'_{WD},v'_{dM}) is the sum of the absolute orbital velocity of that component

(v_{WD},v_{dM}) and the system velocity (γ; see Morgan et al. 2012). Assuming that the binaries are in circular, edge-on orbits, we can combine the component radial velocities with each stars' mass to derive a lower limit on the orbital radial velocity. Uncertainties on these velocities were calculated using standard error propagation techniques. We stress that the orbital velocities derived based on these assumptions are lower limits and should only be used for statistical comparison. To estimate each star's projected distance from the system center-of-mass, we assumed each of the component's absolute orbital velocities is its real orbital velocity. We then summed those values to estimate the total binary separation for each system. We use these projected separations in a comparative way to investigate how magnetic activity changes with binary separation in Section 4.2.
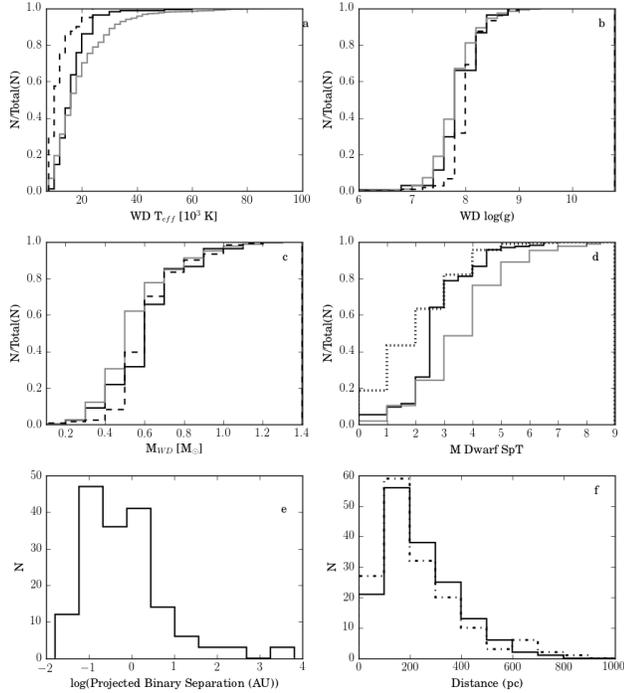
3.4. *Individual Objects*

Figure 3. Cumulative histograms are shown in panels a-d for WD T_{eff}, WD $\log g$, M_{WD}, and M dwarf spectral subtype (SpT). Panels e and f show histograms of binary separation and distance, respectively. In panels a-e, the solid black line shows the newly characterized WD+dMs from SUPERBLINK. The solid gray line in panels a, b, c, and d shows the WD+dM binaries from Rebassa-Mansergas et al. (2013a). The black dashed line shown in panels a-c represents the volume-limited sample of white dwarfs within 20pc from Holberg et al. (2008). The black dotted line in panel d represents the sample of SUPERBLINK single M dwarfs from Gaidos et al. (2014). Panel e shows the distribution in binary separation based on our radial velocity analysis. Panel f shows the spectroscopic distances derived to the M dwarf (solid line) and to the WD (dashdot line).

In our analysis above, we included only WD+dMs containing a DA WD. However, we also did identify two systems with non-DA WD spectral classes. The spectra of these objects are shown in Figure 5. The astrometric and photometric properties are included in Table 1. PM04322-1645 was previously found by Bergeron et al. (2011) as a a DB (Helium-line) WD, but there was no companion identified then. We classified PM09448+8355 as a DAO type (mixed H+He composition) WD due to the presence of HeII $\lambda 4686$ absorption.

4. RESULTS

4.1. *Kinematics*

Combining the stellar positions, estimated radial velocities, spectroscopic distances determined from our M dwarf fits, and the proper motions from the SUPERBLINK catalog, we derived 3D space velocities for each of the WD+dMs in SUPERBLINK (see Table 4). To do this, we made use of the utilities package in `galpy` (Bovy 2015). We accounted for the solar motion relative to the Local Standard of Rest using
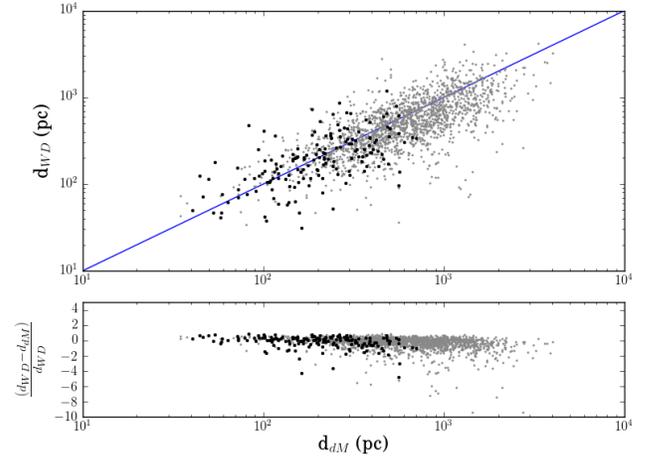

Figure 4. The top panel shows a comparison of the spectroscopic distances estimated for each of the stellar components in the binary. M dwarf distances were determined based on the SpT-M_J relation from Lépine et al. (2013). WD distances were calculated using our best fit parameters and synthetic M_{NUV} magnitudes. Black dots show the newly characterized sample from SUPERBLINK, showing that the SUPERBLINK sample is, on average, closer than the SDSS WD+dM sample (gray dots). The bottom panel shows the difference between each of the distance estimates normalized by the white dwarf distance. In general, the difference in the distance estimates for newly identified SUPERBLINK WD+dMs is similar to differences in distances calculated for the SDSS WD+dMs.
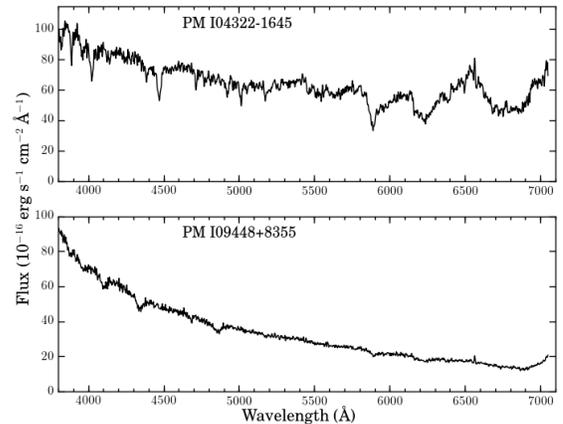

Figure 5. Spectra of the two newly identified systems with non-DA white dwarfs. The top panel shows PM04322-1645, a DB WD previously identified by Bergeron et al. (2011), but no companion was noted. The bottom panel shows PM09448+8355, a system with a DAO WD identified by this work.

values from Schönrich et al. (2010) (11, 12, 7 km s^{-1}). To determine the formal error for each of the space motions, we calculated the covariance matrix for each (U, V, W) vector to propagate the distance, proper motion, and radial velocity uncertainties. The formal error for each object is listed in Table 4. The median uncertainty in each direction (U, V, W) is (20, 16, 32 km s^{-1}) respectively. Figure 6 shows the resulting distributions for each component of the space motion
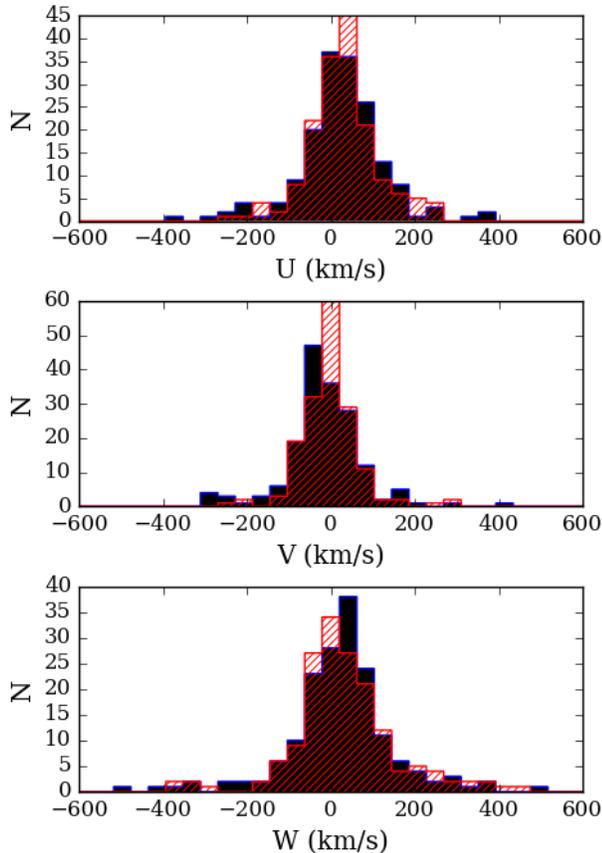
Figure 6. (U, V, W) galactic velocity distributions for the SU-PERBLINK WD+dMs. The velocity distribution for each component for active M dwarfs is shown in hatched red overlaying the distribution for the M dwarfs showing no activity in black.

for the WD+dMs in SUPERBLINK. Stars classified as active are shown in the red, hatched distribution overlaying the distribution for inactive stars in black. Since (for early- to mid-type M dwarfs) active stars should in general be rotating faster and therefore more likely to be from a younger population, we considered three samples for our analysis – the full sample, only the active stars, and only the inactive stars. Under the assumption that the underlying velocity distributions for all three kinematic components are Gaussian, probabilities for a given component's mean (μ) and standard deviation (σ) can be computed analytically and compared to the data using a Bayesian approach. As described in West et al. (2015), we constructed a grid of μ and σ values and explored the joint probability distribution for the three different subsets of the data: 1) all pairs; 2) pairs with an active M dwarf; and 3) pairs with an inactive M dwarf. From the resulting peaks of the joint probability density distributions, we computed μ and σ values for each sub-sample. We also calculated uncertainties from the spread of the marginalized distributions for each parameter. The results of this analysis can be found in Table 4.

Examining the distributions in Figure 6, we find that sys-

tems with inactive M dwarfs have preferentially lower V (azimuthal) velocities, suggesting that the inactive sample is drawn from an older population exhibiting asymmetric drift. This is also reflected in the lower μ_V for the active and inactive distributions. We performed a two-sample Kolmogorov-Smirnov test to compare the active and inactive distributions of V velocities and found a $< 1\%$ chance of being drawn from the same population. This is consistent with results from previous studies (Hawley et al. 1996; Bochanski et al. 2007a), which show that samples of inactive single M dwarfs have more negative V velocities than their active counterparts. We also note that the velocity dispersions in the vertical direction (W) for both active and inactive samples are larger than the velocity dispersions typically associated with the thick disk. Bochanski et al. (2007a) found thick disk velocity dispersions ($\sigma_U, \sigma_V, \sigma W) \approx (50$ km s^{-1}, 40 km s^{-1}, 40 km s^{-1} for K and M dwarfs in SDSS. We attribute this high vertical velocity dispersion to two factors: 1) Selecting M dwarfs with white dwarf companions inherently creates a minimum age limit for our sample since each system must be as old as the progenitor of the white dwarf; and 2) We have preferentially chosen the fast moving systems by selecting these systems using their proper motion. These two effects combined likely produce the observed large vertical velocity dispersion.

4.2. *Magnetic Activity*

Using Hα chromospheric emission as a tracer for magnetic activity, we classified each M dwarf as active or inactive. We integrated over a 12 Å region centered on Hα, with the continuum set by measuring the flux in 5 Å regions on either side of the 12 Å region (West et al. 2004). A star is classified as active if the equivalent width measured is > 1 Å. We visually examined each of the M dwarf component spectra to verify the activity classification. The automatic identification of active systems failed in a number of cases with clear, narrow Hα line emission. Since these systems are close binaries, it is possible that the Hα line moved out of the integrated region. In general, we relied on the visual determination for our analysis. Overall, 55% of our sample was classified as active. Figure 7 shows the activity fraction as a function of spectral type for our sample, as well as WD+dMs from Morgan et al. (2012), single M dwarfs from SUPERBLINK (Gaidos et al. 2014), and single M dwarfs from the Palomar-Michigan State University (PMSU) survey of nearby M dwarfs (Reid et al. 1995; Hawley et al. 1996). We chose spectral type bins representing early, mid and late type M dwarfs. The binary sample from SUPERBLINK, as well as the Morgan et al. (2012) sample show higher activity fractions at early and mid-spectral types compared with the samples of single M dwarfs. Using the observed activity fractions for M dwarfs from SDSS DR5 and a simple 1D dynamical model, West et al. (2008) showed that M0-M2 dwarfs have activity lifetimes ranging from 0.8-1.2 Gyr, mid-M dwarfs (M3-M4)
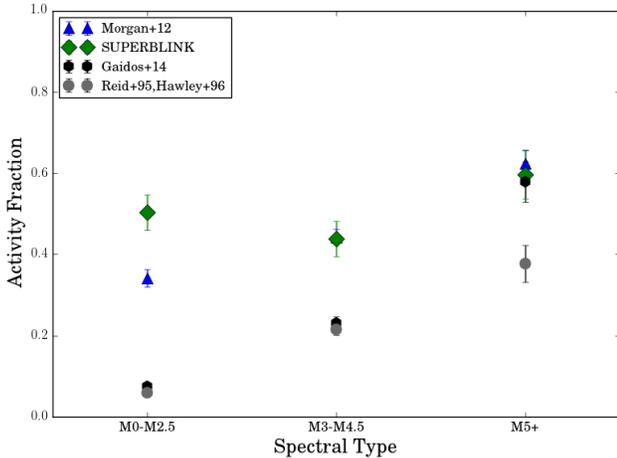
Figure 7. The fraction of active stars as a function of spectral type is shown for the full SUPERBLINK sample of WD+dMs (green diamonds), the WD+dMs from Morgan et al. (2012) (blue triangles) and the samples of nearby single M dwarfs from Gaidos et al. (2014) (black hexagons) and the PMSU survey (Hawley et al. 1996; gray circles). Errors were drawn from the binomial distribution for each sample. The SUPERBLINK WD+dMs and the SDSS WD+dMs show high activity fractions compared to the single M dwarfs at spectral types earlier than M5. At late types, the difference between activity fractions for single stars and WD+dMs decreases or disappears entirely.

Figure 8. Activity fractions for the SUPERBLINK WD+dMs are shown based on our estimated projected binary separations and compared to the same single M dwarf samples as Figure 7. Errors were again drawn from the binomial distribution. Separation bins were chosen based on definitions given by Willems & Kolb (2004). Close separations (a ≤ 0.88 AU) are shown as green triangles, intermediate separation (0.88 AU < a ≤ 2.57 AU) are shown as red squares, and wider systems (a > 2.57 AU) are shown as blue diamonds. For early-type systems, WD+dMs at all separations have higher activity fractions than the samples of single stars. For mid-types, the activity fraction for the widest system matches that of the sample of single M dwarfs hinting that there may be a threshold where the binary companion plays a less significant role. At late types, the active fraction does not vary much with separation, but we note that we have the fewest objects in the late-type bin.

have activity lifetimes 2-4 Gyr, and late M dwarfs (M5-M6) have activity lifetimes 7-8 Gyr. For these binaries with early or mid-type M dwarfs, the high activity fractions compared to single M dwarf samples indicates that the companion likely plays an important role in lengthening the activity lifetime. For systems with late-type M dwarf components, both binary samples show higher activity fractions than the PMSU survey, but are the same as the Gaidos et al. (2014) sample. Also selected from SUPERBLINK, the M dwarfs from Gaidos et al. (2014) however all have $J < 9$; this magnitude limit may introduce a selection bias toward younger M dwarfs that would have the largest effect for the latest M spectral types.

We investigated the effects that binary separation could have on the activity fraction in our sample as compared to single stars. Figure 8 shows the activity fractions for our sample binned by their likelihood of having gone through common envelope evolution. For this, we used the orbital period bins derived for white dwarf main sequence binaries by Willems & Kolb (2004). For early-type M dwarfs in WD+dMs, we continue to see high activity fractions across all binary separations. For mid-type WD+dMs with wider separations, the activity fraction for WD+dMs matches that of the single M dwarf populations. At these wider separations, the binary companion may not significantly affect the activity lifetimes for this population of stars. At closer separations, we continue to see high activity fractions indicating longer activity lifetimes for mid-type M dwarfs with close companions. At late spectral types, we see high activity fractions at all projected binary separations. We note that
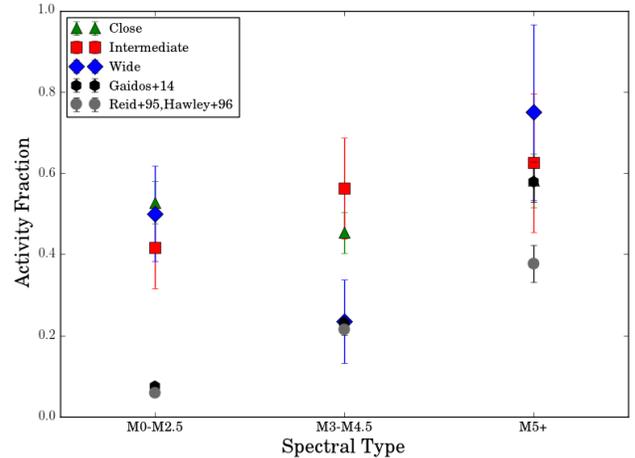
our sample contains relatively few late-type M dwarfs with WD companions, so further investigation is needed to understand how binary separation may affect the activity lifetimes of late-type M dwarfs with binary companions.

Since WD+dM systems contain the remnant of an evolved star, the M dwarfs in these systems are likely older than the complementary samples of nearby single M dwarfs and M dwarfs with main sequence companions (see also Section 4.1). Using the initial-final mass function for WDs from Kalirai et al. (2008) combined with our median WD mass (0.62 M$_\odot$), we estimate that the most likely mass of a white dwarf progenitor for our sample of WD+dMs is 2.07 M$_\odot$. Typically, 2 M$_\odot$ stars have main sequence lifetimes of ~1 Gyr (Paxton et al. 2010). Comparing this to the activity lifetimes derived by West et al. (2008), most of the M0-M2 dwarfs in WD+dMs should be older than what their single M dwarf activity lifetimes might suggest (i.e. their single star counterparts of similar age should be mostly inactive). This is further evidence that a close companion prolongs the activity lifetimes in the stars in a significant way. As outlined in section 1, tidal effects play a role in keeping the M dwarfs in the closest binaries rotating quickly. In particular, Rebassa-Mansergas et al. (2013b) showed that all of the M dwarfs in a sample of confirmed post-common envelope binaries were active. We also see high activity fractions for binaries at intermediate separations. The physical mechanism behind this

is less clear, but may be related to early inhibition of angular momentum loss through disk disruption or dissipation.

5. CONCLUSION

We have identified and characterized WD+dMs selected from the SUPERBLINK proper motion survey. It is the first catalog of WD+dMs for which all objects have well-measured proper motions, enabling a first look at the Galactic kinematics of these objects. We used the presence of Hα to investigate the effects of a close WD companion on M dwarf magnetic activity fractions. We compared the M dwarf activity fractions for the SUPERBLINK WD+dMs and SDSS DR8 WD+dMs to nearby samples of single M dwarfs and examined how activity fraction changes with projected binary separation. We summarize our findings below:

1. We used a UV-Optical-IR color selection to select for WD+dMs in the SUPERBLINK proper motion survey. Spectroscopic follow-up at MDM Observatory yielded 178 previously uncharacterized systems. Combined with previously identified binaries, we now have confirmed 470 nearby WD+dMs in the SUPERBLINK proper motion survey to date.

2. We fit each of our spectra with WD models and M dwarf templates to derive the physical parameters of each of the stars in the WD+dM binaries. Output parameters of these fits include WD effective temperature and gravity, M dwarf spectral type, lower limits on the radial velocities, approximate binary separations, magnetic activity (traced by Hα). Combined with synthetic absolute NUV photometry for the WDs, we calculated a spectroscopic distance to the WD in each system. Using a Spt-M_J relation, we calculate a spectroscopic distance to the M dwarf in each system. We found that the SUPERBLINK sample is on average significantly closer than previous samples of WD+dMs identified from SDSS.

3. Combining the proper motions from SUPERBLINK with each WD+dM position, estimated radial velocity, and M dwarf spectroscopic distance, we calculated 3D space velocities. We found evidence for asymmetric drift in the binaries containing inactive M dwarfs, indicating this subsample is likely drawn from an older population than the systems with active M dwarfs. We also found that the entire sample has a vertical (W) velocity dispersion larger than that of local field stars, suggesting the entire sample is drawn from an older population of stars than the complementary high proper motion samples of single M dwarfs.

4. The magnetic activity fraction for M dwarfs in the SUPERBLINK WD+dM sample corroborates previous findings that the activity fraction in these binaries is higher for early- and mid-M dwarfs than for samples of single M dwarfs. At late spectral types, this difference in activity fraction decreases or disappears.

5. We examined how activity fraction changes as a function of binary separation and found enticing evidence of a limiting separation where the existence of a companion does not affect the activity fraction of a sample of mid-M dwarfs. For early spectral types, we found high activity fractions at each of our separation bins. For mid-spectral types, we found high activity fractions for systems with close and intermediate separations. At wide separations, however, activity fraction for the binaries matched the single star populations suggesting a separation threshold where companions do not contribute to higher activity fraction.

This work, combined with the evidence from previous studies of WD+dMs, highlights the need to define three distinct separation regimes for understanding how M dwarfs (and stars in general) are affected by evolved companions. Categories of binaries are usually restricted to "close", where interactions dominate and change the evolution of the two stars and "wide", where each component is assumed to evolve as a single star. However, we argue that an intermediate separation category should be used, as we clearly find evidence for higher activity fractions at projected separations outside the regime of tidal interaction. Higher activity fractions indicate longer activity lifetimes and therefore longer spindown times. To achieve this, there must be some inhibition of angular momentum loss either at early epochs via disk disruption or dissipation or throughout the binary lifetime via magnetic field locking. Meibom et al. (2007) interpreted shorter binary primary rotation periods for solar-type stars in a young open cluster (M35) as the result of early disk disruption or dissipation. Disk disruption or dissipation may cause binaries to follow a delayed Skumanich-type (Skumanich 1972) power law, where spindown is delayed compared to single stars. A difference in the normalization of the Skumanich-type relation has been argued previously in the more extreme case of cataclysmic variables (Patterson 1984; Knigge et al. 2011). It is also possible that the M dwarf spindown is altered by the presence of the white dwarf magnetic field. Cohen et al. (2012) showed that the extreme case of a magnetic cataclysmic variable, the presence of a strong white dwarf magnetic field could reduce the M dwarf outflow by reducing open field regions. More work is needed to understand how binaries outside the regime of tidal interactions may be affected by magnetic field interactions.

Comparison to other binaries containing M dwarfs and other main sequence stars is needed to fully understand the effects of the white dwarf progenitor's evolution. However, WD+dMs remain useful probes of how close companions affect the magnetic activity of M dwarfs, largely due to their bright and spectroscopically distinct nature.

REFERENCES

Bergeron, P., Wesemael, F., Dufour, P., et al. 2011, ApJ, 737, 28

Bochanski, J. J., Hawley, S. L., & West, A. A. 2011, AJ, 141, 98

Bochanski, J. J., Munn, J. A., Hawley, S. L., et al. 2007a, AJ, 134, 2418

Bochanski, J. J., West, A. A., Hawley, S. L., & Covey, K. R. 2007b, AJ, 133, 531

Bovy, J. 2015, ApJS, 216, 29

Chabrier, G., & Baraffe, I. 1997, A&A, 327, 1039

Cohen, O., Drake, J. J., & Kashyap, V. L. 2012, ApJ, 746, L3

Delfosse, X., Forveille, T., Perrier, C., & Mayor, M. 1998, A&A, 331, 581

Duchêne, G., & Kraus, A. 2013, ARA&A, 51, 269

Farihi, J., Becklin, E. E., & Zuckerman, B. 2005, ApJS, 161, 394

Farihi, J., Hoard, D. W., & Wachter, S. 2006, ApJ, 646, 480

Feiden, G. A. 2015, Living Together: Planets, 496, 137

Gaidos, E., Mann, A. W., Lépine, S., et al. 2014, MNRAS, 443, 2561

Ghosh, P., & Lamb, F. K. 1979, ApJ, 232, 259

Gizis, J. E., Reid, I. N., & Hawley, S. L. 2002, AJ, 123, 3356

Hawley, S. L., Gizis, J. E., & Reid, I. N. 1996, AJv.112, 112, 2799

Heller, R., Homeier, D., Dreizler, S., & Østensen, R. 2009, A&A, 496, 191

Hoard, D. W., Wachter, S., Sturch, L. K., et al. 2007, AJ, 134, 26

Holberg, J. B., & Bergeron, P. 2006, AJ, 132, 1221

Holberg, J. B., Sion, E. M., Oswalt, T., et al. 2008, AJ, 135, 1225

Hunter, J. D. 2007, Computing In Science & Engineering, 9, 90

Kalirai, J. S., Hansen, B. M. S., Kelson, D. D., et al. 2008, ApJ, 676, 594

Kiraga, M., & Stepien, K. 2007, Acta Astronomica, 57, 149

Knigge, C., Baraffe, I., & Patterson, J. 2011, ApJS, 194, 28

Koester, D., Napiwotzki, R., Christlieb, N., et al. 2001, A&A, 378, 556

Kowalski, P. M., & Saumon, D. 2006, ApJ, 651, L137

Lanning, H. H. 1982, ApJ, 253, 752

Lawrence, A., Warren, S. J., Almaini, O., et al. 2007, MNRAS, 379, 1599

Lépine, S., & Gaidos, E. 2011, AJ, 142, 138

Lépine, S., Hilton, E. J., Mann, A. W., et al. 2013, AJ, 145, 102

Lépine, S., & Shara, M. M. 2005, AJ, 129, 1483

Lépine, S., Shara, M. M., & Rich, R. M. 2002, AJ, 124, 1190

Li, L., Zhang, F., Han, Q., Kong, X., & Gong, X. 2014, MNRAS, 445, 1331

Limoges, M. M., Lépine, S., & Bergeron, P. 2013, AJ, 145, 136

Liu, C., Li, L., Zhang, F., et al. 2012, MNRAS, 424, 1841

Margon, B., Liebert, J., Lampton, M., et al. 1976, ApJ, 209, 525

Martin, D. C., Fanson, J., Schiminovich, D., et al. 2005, ApJ, 619, L1

Matt, S., & Pudritz, R. E. 2005, MNRAS, 356, 167

Meibom, S., Mathieu, R. D., & Stassun, K. G. 2007, ApJ, 665, L155

Mohanty, S., & Basri, G. 2003, ApJ, 583, 451

Morgan, D. P., West, A. A., Garcés, A., et al. 2012, AJ, 144, 93

Nebot Gomez-Moran, A., Gänsicke, B. T., Schreiber, M. R., et al. 2011, A&A, 536, A43

Østensen, R. H., Silvotti, R., Charpinet, S., et al. 2010, MNRAS, 409, 1470

Patterson, J. 1984, ApJS, 54, 443

Paxton, B., Bildsten, L., Dotter, A., et al. 2010, ApJS, 192, 3

Raymond, S. N., Szkody, P., Hawley, S. L., et al. 2003, AJ, 125, 2621

Rebassa-Mansergas, A., Agurto-Gangas, C., Schreiber, M. R., Gänsicke, B. T., & Koester, D. 2013a, MNRAS, 433, 3398

Rebassa-Mansergas, A., Gänsicke, B. T., Schreiber, M. R., Koester, D., & Rodríguez-Gil, P. 2010, MNRAS, 402, 620

Rebassa-Mansergas, A., Ren, J. J., Parsons, S. G., et al. 2016, MNRAS, 458, 3808

Rebassa-Mansergas, A., Schreiber, M. R., & Gänsicke, B. T. 2013b, MNRAS, 429, 3570

Rebassa-Mansergas, A., Zorotovic, M., Schreiber, M. R., et al. 2012, MNRAS, 423, 320

Reid, I. N., & Hawley, S. L. 2005, New light on dark stars : red dwarfs, low-mass stars, brown dwarfs, doi:10.1007/3-540-27610-6

Reid, I. N., Hawley, S. L., & Gizis, J. E. 1995, AJv.110, 110, 1838

Reiners, A., & Basri, G. 2007, ApJ, 656, 1121

Ren, J. J., Rebassa-Mansergas, A., Luo, A. L., et al. 2014, A&A, 570, A107

Schönrich, R., Binney, J., & Dehnen, W. 2010, MNRAS, 403, 1829

Schreiber, M. R., & Gänsicke, B. T. 2003, A&A, 406, 305

Shu, F., Najita, J., Ostriker, E., et al. 1994, ApJ, 429, 781

Silvestri, N. M., Hawley, S. L., West, A. A., et al. 2006, AJ, 131, 1674

Silvestri, N. M., Lemagie, M. P., Hawley, S. L., et al. 2007, AJ, 134, 741

Skinner, J. N., Thorstensen, J. R., & Lépine, S. 2014, AJ, 148, 1

Skrutskie, M. F., Cutri, R. M., Stiening, R., et al. 2006, AJ, 131, 1163

Skumanich, A. 1972, ApJ, 171, 565

Tappert, C., Gänsicke, B. T., Schmidtobreick, L., Mennickent, R. E., & Navarrete, F. P. 2007, A&A, 475, 575

The Astropy Collaboration, Robitaille, T. P., Tollerud, E. J., et al. 2013, A&A, 558, A33

Tremblay, P. E., Bergeron, P., & Gianninas, A. 2011, ApJ, 730, 128

Voges, W., Aschenbach, B., Boller, T., et al. 1999, A&A, 349, 389

Voges, W., Aschenbach, B., Boller, T., et al. 2000, IAUC, 7432

Wachter, S., Hoard, D. W., Hansen, K. H., et al. 2003, ApJ, 586, 1356

Warren, S. J., Hambly, N. C., Dye, S., et al. 2007, MNRAS, 375, 213

West, A. A., Hawley, S. L., Bochanski, J. J., et al. 2008, AJ, 135, 785

West, A. A., Weisenburger, K. L., Irwin, J., et al. 2015, ApJ, 812, 1

West, A. A., Hawley, S. L., Walkowicz, L. M., et al. 2004, AJ, 128, 426

Willems, B., & Kolb, U. 2004, A&A, 419, 1057

Wright, E. L., Eisenhardt, P. R. M., Mainzer, A. K., et al. 2010, AJ, 140, 1868

York, D. G., Adelman, J., Anderson, J. E. J., et al. 2000, AJ, 120, 1579

Table 1. Astrometric and Photometric Properties of the WD+dMs in the SUPERBLINK proper motion survey

Name	RA (J2000.0)	Dec (J2000.0)	$[\mu_\alpha, \mu_\delta]$ (mas yr^{-1})	FUV mag	NUV mag	V mag	J mag	H mag	K_s mag	NUV-V	V-K_s	Type[a]	Reference
PM I00010+3527	0.274231	35.461109	[46.0,1.0]	18.97	19.05	17.96	15.17	14.58	14.25	1.09	3.71	DA/M	This Work
PM I00057+2915	1.445243	29.260513	[-51.0,-58.0]	...	...	18.31	16.78	15.41	15.34	...	2.97	DA/M:	RM12
PM I00090+4348	2.268687	43.81242	[70.0,-35.0]	18.57	17.92	16.77	13.69	13.05	12.81	1.15	3.96	DA/M	This Work
PM I00136+0019	3.413117	0.323517	[406.0,-188.0]	19.70	16.42	15.62	15.15	15.21	15.1	0.8	0.52	(WD/M)	RM12
PM I00139-1108E	3.497771	-11.144092	[24.0,32.0]	17.50	17.79	16.12	13.49	12.85	12.7	1.67	3.42	DA/M	RM12,M12
PM I00219-1103	5.491246	-11.058861	[-6.0,-44.0]	21.95	19.71	18.15	14.84	14.37	14.03	1.56	4.12	DA/M	RM12,M12
PM I00241+0548	6.030123	5.815727	[134.0,-30.0]	18.34	17.34	16.26	12.73	12.15	11.88	1.08	4.38	DA/M	This Work
PM I00263+1444	6.585003	14.735963	[22.0,-34.0]	17.14	17.31	17.15	14.68	14.16	13.92	0.16	3.23	DA/M	RM12,M12
PM I00278-0010	6.958331	-0.17318	[63.0,-11.0]	20.00	18.73	18.04	15.01	14.65	14.29	0.69	3.75	DB/M	RM12,M12
PM I00305+0706	7.637668	7.116136	[35.0,-51.0]	18.13	17.86	17.93	...	...	...	-0.07	...	(DA/M)	RM12
PM I00336+0041	8.402044	0.697649	[-41.0,-61.0]	...	...	19.39	15.11	14.41	14.15	...	5.24	WD/M	RM12
PM I00342+0004	8.555728	0.07724	[75.0,-17.0]	...	...	17.82	15.06	14.54	14.22	...	3.6	WD/M	RM12
PM I00365+1118	9.145305	11.302482	[-55.0,-23.0]	17.44	17.42	17.86	16.66	15.87	16.38	-0.44	1.48	(WD/M)	This Work
PM I00380+0834	9.51839	8.571456	[2.0,-55.0]	23.07	20.29	17.83	13.98	13.46	13.2	2.46	4.63	DA/M	RM12,M12
PM I00389+0106	9.736704	1.114177	[-29.0,-46.0]	...	...	18.65	14.67	14.01	13.71	...	4.94	WD/M	RM12,M12

[a]Types of WD+dMs are given according to the convention outlined in Rebassa-Mansergas et al. (2010). For objects found in both SDSS and SUPERBLINK, we have used the types given by the catalogue maintained at http://sdss-wdms.org/. A colon after a component type indicates the classification of that component is uncertain. Parentheses indicate that the system is a WD+dM candidate. More details about these classifications can be found in Rebassa-Mansergas et al. (2010).

References—F05 - Farihi et al. (2005), F06 - Farihi et al. (2006), H07 - Hoard et al. (2007), L82 - Lanning (1982), L14 - Li et al. (2014), L13 - Limoges et al. (2013), M76 - Margon et al. (1976), M12 - Morgan et al. (2012), O10 - Østensen et al. (2010), RM12 - Rebassa-Mansergas et al. (2012), R14 - Ren et al. (2014), T07 - Tappert et al. (2007), W03 - Wachter et al. (2003)

Table 2. Spectral Types, Radial Velocities, and Spectroscopic Distances of the newly identified SUPERBLINK WD+dMs

Name	dM SpT	WD T_{eff} (K)	WD $log(g)$	WD RV (km s^{-1})	$\sigma_{WD\,RV}$ (km s^{-1})	dM RV (km s^{-1})	$\sigma_{dM\,RV}$ (km s^{-1})	System RV (km s^{-1})	$\sigma_{sys\,RV}$ (km s^{-1})	Separation (AU)	Activity Flag	dM Distance (pc)	WD Distance (pc)
PM I00010+3527	M3.0	16000.0	8.25	93.1	301.2	142.0	104.4	-100.0	54.6	.08	1	389.2	340.3
PM I00090+4348	M3.0	14000.0	7.75	240.3	101.0	208.3	90.7	-50.7	81.7	.02	1	196.9	220.3
PM I00241+0548	M2.0	16000.0	7.5	72.7	186.5	144.0	118.8	32.4	66.4	.12	1	205.5	251.1
PM I00554-0831	M6.5	14000.0	8.0	79.0	56.8	-51.7	214.3	-63.9	17.6	.15	0	79.3	114.3
PM I01103-1853E	M3.5	10000.0	7.75	54.7	95.7	59.3	47.9	-16.8	46.5	.27	0	177.4	162.7
PM I01163-0436	M2.5	35000.0	8.0	38.3	89.2	40.6	46.6	12.5	42.8	.58	0	487.0	448.5
PM I01187+0505	M2.5	14000.0	7.75	291.3	148.3	-21.3	148.3	83.9	109.0	.79	1	310.1	197.3
PM I01230-1750	M2.0	16000.0	8.0	262.6	111.2	-94.8	117.7	45.9	31.5	.04	1	200.8	143.4
PM I01269+7202	M2.5	25000.0	7.75	16.0	124.2	-1.8	58.0	-76.3	.9	108.54	1	310.1	291.5
PM I01345+2102	M3.0	12000.0	7.75	154.1	180.7	-116.9	132.7	25.5	36.6	.05	1	101.9	185.2
PM I01459+2041	M4.0	14000.0	8.0	-25.2	181.5	243.9	97.6	-25.5	69.9	.84	0	182.6	114.9
PM I02016-1838	M4.5	14000.0	8.0	-23.9	74.9	215.6	154.9	-17.2	38.9	.94	1	73.2	86.7
PM I02071-1543	M2.5	13000.0	7.75	110.7	147.9	-11.3	54.3	17.3	52.2	2.82	0	91.5	81.9
PM I02113+1212	M2.5	16000.0	8.0	106.5	175.1	-196.9	262.1	34.7	40.9	.06	0	372.8	547.8
PM I02154+1440	M2.5	11000.0	8.5	145.3	83.7	46.1	102.6	23.3	55.4	.19	1	569.5	138.9

Table 3. 3D Space Velocities for SUPERBLINK WD+dMs

Name	U (km s^{-1})	σ_U (km s^{-1})	V (km s^{-1})	σ_V (km s^{-1})	W (km s^{-1})	σ_W (km s^{-1})
PM I00010+3527	32.71	22.05	-98.91	46.1	39.75	26.0
PM I00090+4348	20.63	33.31	-59.2	70.52	-15.0	26.9
PM I00139-1108E	73.67	14.63	97.54	26.84	-186.39	75.48
PM I00219-1103	20.72	4.41	23.08	20.57	-127.08	64.3
PM I00241+0548	64.88	15.71	-36.4	36.07	-49.39	55.55
PM I00263+1444	44.58	21.1	72.31	47.35	-101.82	56.86
PM I00278-0010	69.86	15.93	35.57	36.26	-125.49	73.63
PM I00380+0834	-11.93	39.26	-54.12	75.92	25.07	117.94
PM I00389+0106	55.55	32.3	147.56	64.98	-326.07	133.56
PM I00532-0032	-5.73	23.41	57.59	36.07	-223.19	80.77
PM I00554-0831	18.17	4.85	-20.29	5.54	67.23	16.69
PM I01101+1326	106.44	29.04	83.36	34.55	-142.4	52.02
PM I01103-1853E	-31.6	10.13	-14.76	7.08	16.01	45.94
PM I01106-0108	67.16	13.24	35.63	13.98	-151.54	28.98
PM I01163-0436	-64.5	21.43	-1.8	17.02	-34.79	39.93

Table 4. Population Kinematics

Pop. ID	μ_u	μ_v	μ_w	σ_u	σ_v	σ_w
All	$20.6^{3.8}_{3.7}$	$-12.6^{2.9}_{2.9}$	$24.2^{4.2}_{4.2}$	$72.3^{3.4}_{3.2}$	$54.6^{2.7}_{2.6}$	$85.2^{3.8}_{3.6}$
Active	$21.2^{4.5}_{4.4}$	$-6.4^{3.3}_{3.3}$	$24.8^{5.8}_{5.4}$	$60.6^{3.9}_{3.5}$	$42.9^{3.1}_{2.9}$	$88.7^{4.7}_{4.4}$
Inactive	$19.2^{5.9}_{5.9}$	$-19.3^{4.8}_{4.8}$	$23.7^{5.5}_{5.5}$	$85.6^{5.5}_{5.1}$	$65.7^{4.5}_{4.2}$	$79.9^{5.4}_{5.0}$